JOURNAL OF MATERIALS SCIENCE 9 (1974) 591–606

Viscoelastic behaviour of a unidirectional fibre reinforced plastic

EIRYO SHIRATORI, KOZO IKEGAMI, TOSHIO HATTORI
Research Laboratory of Precision Machinery and Electronics, Tokyo Institute of Technology, Tokyo, Japan

The orthogonal linear viscoelastic constitutive equation is given by the Laplace transform domain elastic constants which are calculated from the law of mixture and a structural unit cell. Non-linear constitutive relations in high stress regions are derived by considering non-linear properties of the components and the stress redistribution in the matrix on account of debonding between fibre and matrix. A linear failure criterion and a fracture criterion are also investigated theoretically. Experimental works are conducted for uniaxial and biaxial specimens of cold-drawn copper fibre-epoxy resin composite having various fibre volume fractions and fibre directions. Fairly good agreements are observed between the calculated and experimental results.

1. Introduction

It is well known that the fibre reinforced composite material shows a considerable mechanical anisotropy depending on the orientation and volume fraction of fibres. From this variability of anisotropy by fibre reinforcement, it is possible to choose the optimal reinforcement from the view point of material efficiency of the composite material for the prescribed design condition. For optimal design by use of composite material, it is necessary to find the constitutive relation of composite material. Although many papers have reported on this problem, there are few theoretical and experimental results for the constitutive relation from the start of deformation to the fracture of the composite. Moreover, since the results are often given by complicated expressions or numerical calculations with digital computers, they are not always convenient for stress analysis of the structures.

It is a main object of this paper to find the simple and approximately precise expression of constitutive relation which is available for the design purpose. Theoretical analyses are made on the linear and non-linear viscoelastic anisotropic behaviour, linear viscoelastic failure and fracture criteria for uniaxial fibre reinforced composite. The validity of the analytical results is confirmed by comparison with the experimental results.

2. Linear viscoelastic behaviour

Let us assume that the matrix is a time-dependent material and the fibres embedded in the matrix are elastic materials. The macroscopic property of the composite will then be time dependent, and it will show a linear viscoelastic behaviour within a low strain region. It is well known that a linear viscoelastic problem can be solved by the correspondence principle as an associated elastic problem in the Laplace transform domain. Accordingly, the orthotropic linear viscoelastic constitutive equation for the composite composed of linear viscoelastic matrix and parallel elastic fibres can be determined by the Laplace transform inversion of associated orthotropic elastic constants.

The constitutive equation in the Laplace transform domain of an orthotropic elastic plate, in the case of plane stress condition where the stress co-ordinate axes coincide with the principal axes of anisotropy, is defined as follows:

$$\begin{pmatrix} \bar{\epsilon}_{11} \\ \bar{\epsilon}_{22} \\ \bar{\gamma}_{12} \end{pmatrix} = \begin{pmatrix} 1/\bar{E}_{11} & 1/\bar{E}_{12} & 0 \\ 1/\bar{E}_{12} & 1/\bar{E}_{22} & 0 \\ 0 & 0 & 1/\bar{G}_{12} \end{pmatrix} \begin{pmatrix} \bar{\sigma}_{11} \\ \bar{\sigma}_{22} \\ \bar{\tau}_{12} \end{pmatrix} \quad (1)$$

where subscripts 11 and 22 show the directions parallel and perpendicular to fibres respectively (cf. Fig. 1), and the bar indicates the Laplace transformation. For the case where the

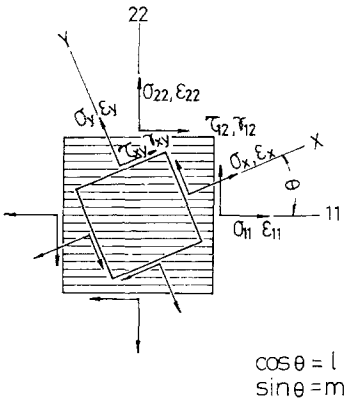

Figure 1 Co-ordinate system of unidirectional fibre reinforced plate.

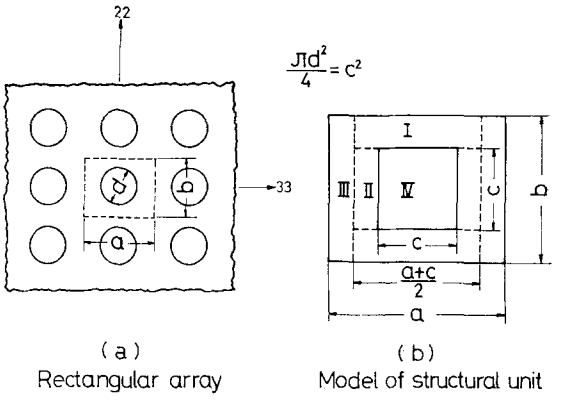

Figure 2 Structural unit cell for the unidirectional fibre reinforced composite of rectangular array.

fibre direction makes an angle θ with one of the stress co-ordinate axis, X, the constitutive equation can be derived from the transformation of the co-ordinates in Equation 1. The elastic compliance matrix of Equation 1 corresponds to the viscoelastic compliance matrix in the physical domain. The associated elastic constants $\bar{E}_{11}$, $\bar{E}_{12}$, $\bar{E}_{22}$, $\bar{G}_{12}$ are determined from elastic moduli of the fibre ($\bar{E}_f$) and the matrix ($\bar{E}_m$) in the Laplace transform domain, fibre volume fraction (V_f) and geometrical arrangements of fibres.

2.1. $\bar{E}_{11}$

According to many analyses and experiments [1-4] the "law of mixture" can be used for the longitudinal modulus with sufficient exactness, i.e.,

$$\bar{E}_{11} = V_f\bar{E}_f + (1 - V_f)\bar{E}_m . \qquad (2)$$

2.2. $\bar{E}_{12}$

For the Poisson's ratio $\bar{\nu}_{12}$ the validity of the law of mixture is verified also in [2, 4], hence

$$\bar{E}_{12} = -\frac{\bar{E}_{11}}{\bar{\nu}_{12}} = -\frac{V_f\bar{E}_f + (1 - V_f)\bar{E}_m}{V_f\bar{\nu}_f + (1 - V_f)\bar{\nu}_m} , \qquad (3)$$

where $\bar{\nu}_f$ and $\bar{\nu}_m$ are the Poisson's ratios of fibre and matrix in the Laplace transform domain defined by

$$\bar{\nu}_m = -\frac{\bar{\epsilon}_{mt}}{\bar{\epsilon}_m} , \quad \bar{\nu}_f = -\frac{\bar{\epsilon}_{ft}}{\bar{\epsilon}_f} . \qquad (4)$$

Here ϵ_m and ϵ_{mt} denote the strains in the directions parallel and perpendicular to the loading direction under uniaxial tensile creep of matrix respectively, and ϵ_f and ϵ_{ft} are those for the fibre.

2.3. $\bar{E}_{22}$

Many results [4-15] have been obtained for the transverse modulus ($\bar{E}_{22}$), but the results are not always convenient for the stress analysis of the structures as they are given by complicated expressions or numerical tables. A simple and approximately precise expression of the transverse modulus is derived from assuming a structural unit cell as shown in Fig. 2 for a rectangular array composite. Fig. 2a shows a cross-section of the composite. The structural unit cell is the rectangular prism of sides $a \times b$ having a fibre of diameter d in the centre, as shown by the dotted lines in Fig. 2a. The unit cell is divided into four regions, and the strain distribution in each region is assumed to be approximately uniform. These four regions are denoted as I, II, III and IV as shown in Fig. 2b. As the cross-sectional area of the region IV must be equal to that of fibre, i.e.,

$$\frac{\pi d^2}{4} = c^2 \text{ and } V_f = c^2/ab .$$

For the tensile loading in direction 22, the equilibriums of stress among these regions are assumed as follows:

(i) the stress of direction 22 in region I is equal to the average stress of regions II and IV, i.e.,

$$\frac{2c}{a + c}\bar{\sigma}_{22}^{IV} + \frac{a - c}{a + c}\bar{\sigma}_{22}^{II} = \bar{\sigma}_{22}^{I} ; \qquad (5)^*$$

(ii) the average stress of regions I and III is equal to the macroscopical stress ($\bar{\sigma}_{22}$) of direction 22, i.e.,

*The stresses in regions I, II, III and IV are denoted by σ^I, σ^{II}, σ^{III} and σ^{IV}, respectively.

$$\frac{a+c}{2a}\bar{\sigma}_{22}{}^{\mathrm{I}} + \frac{a-c}{2a}\bar{\sigma}_{22}{}^{\mathrm{III}} = \bar{\sigma}_{22}\,; \qquad (6)$$

(iii) the macroscopical stress of direction 11 is zero, i.e.,

$$\frac{(a+c)(b-c)}{2}\bar{\sigma}_{11}{}^{\mathrm{I}} + \frac{b(a-c)}{2}\bar{\sigma}_{11}{}^{\mathrm{III}} + c^2\bar{\sigma}_{11}{}^{\mathrm{IV}} = 0\,. \qquad (7)$$

In Equation 7, the stress of region II ($\sigma_{11}{}^{\mathrm{II}}$) is not taken into consideration because of its small value compared with the stresses in other regions.

For the above mentioned loading, the compatibility of the strain among the regions are assumed as follows:

(i) the strains of direction 22 in regions II and IV are equal because of the perfect bonding between fibre and matrix, i.e.,

$$\bar{\epsilon}_{22}{}^{\mathrm{II}} = \bar{\epsilon}_{22}{}^{\mathrm{IV}}\,; \qquad (8)$$

(ii) the strain of direction 22 in region III is equal to the average strain of regions I, II and IV and correspond to the macroscopic strain ($\bar{\epsilon}_{22}$), i.e.,

$$\frac{b-c}{b}\bar{\epsilon}_{22}{}^{\mathrm{I}} + \frac{c}{b}\bar{\epsilon}_{22}{}^{\mathrm{II}} = \bar{\epsilon}_{22}{}^{\mathrm{III}} = \bar{\epsilon}_{22}\,; \qquad (9)$$

(iii) the strains of direction 11 in regions I, III and IV are equal to each other, i.e.,

$$\bar{\epsilon}_{11}{}^{\mathrm{I}} = \bar{\epsilon}_{11}{}^{\mathrm{III}} = \bar{\epsilon}_{11}{}^{\mathrm{IV}}\,, \qquad (10)$$

where the strain of direction 11 in region II ($\bar{\epsilon}_{11}{}^{\mathrm{II}}$) is neglected for the same reason stated for Equation 7. From Equations 5 to 10 the transform domain transverse modulus $\bar{E}_{22}$ is given by

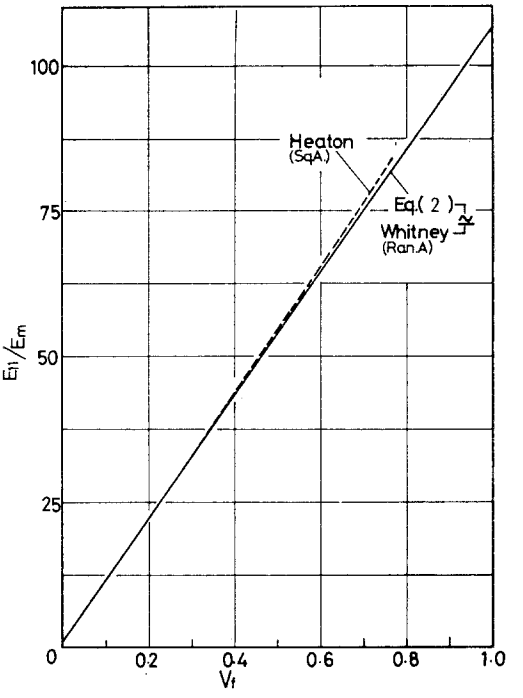

Figure 3 Comparison of calculated results from Equation 2 and from Whitney [2] and Heaton [12].

2.4. $\bar{G}_{12}$

For the longitudinal shear loading, the following equations of the stress equilibrium and strain compatibility among the regions in the unit cell can be derived from the same assumptions as in the case of $\bar{E}_{22}$, i.e.,

$$\bar{E}_{22} = \frac{\bar{\sigma}_{22}}{\bar{\epsilon}_{22}} = \bar{E}_m\left\{1 + \frac{R\dfrac{a+c}{a} + \dfrac{a-c}{a} - 2(1-\bar{\nu}_m{}^2)}{R\dfrac{\bar{E}_m}{\bar{E}_f}\dfrac{(a+c)(b-c)}{c^2} + \dfrac{\bar{E}_m}{\bar{E}_f}\dfrac{(a-c)}{c^2} + 2(1-\bar{\nu}_m{}^2)}\right\} \qquad (11)$$

where

$$R = \frac{\left(1 - \dfrac{(a+c)\bar{E}_m}{2c\bar{E}_f + (a-c)\bar{E}_m}\right)\dfrac{1}{\bar{E}_f}\left(\dfrac{a-c}{2c}\right) + \dfrac{1-\bar{\nu}_m{}^2}{\bar{E}_m}}{-\dfrac{c}{b}\left(1 - \dfrac{(a+c)\bar{E}_m}{2c\bar{E}_f + (a-c)\bar{E}_m}\right)\left(\dfrac{1}{\bar{E}_m} + \dfrac{1}{\bar{E}_f}\dfrac{(a+c)(b-c)}{2c^2}\right) + \left(1 + \dfrac{c-b}{b}\bar{\nu}_m{}^2\right)\dfrac{1}{\bar{\nu}_m\bar{E}_m}}\,.$$

For $\bar{E}_f \gg \bar{E}_m$, R is reduced to $R = b/(b-c)$ and then,

$$\bar{E}_{22} = \bar{E}_m\left\{1 + \frac{1 + \dfrac{c(a+c)}{a(b-c)} - (1-\bar{\nu}_m{}^2)}{\dfrac{\bar{E}_m}{\bar{E}_f}\dfrac{ab}{c^2} + (1-\bar{\nu}_m{}^2)}\right\}. \qquad (12)$$

$$\frac{2c}{a+c}\bar{\tau}_{12}{}^{\mathrm{IV}} + \frac{a-c}{a+c}\bar{\tau}_{12}{}^{\mathrm{II}} = \bar{\tau}_{12}{}^{\mathrm{I}}, \qquad (13)$$

$$\frac{a+c}{2a}\bar{\tau}_{12}{}^{\mathrm{I}} + \frac{a-c}{2a}\bar{\tau}_{12}{}^{\mathrm{III}} = \bar{\tau}_{12}\,, \qquad (14)$$

$$\bar{\gamma}_{12}{}^{\mathrm{II}} = \bar{\gamma}_{12}{}^{\mathrm{IV}} \qquad (15)$$

$$\frac{b-c}{b}\bar{\gamma}_{12}{}^{\mathrm{I}} + \frac{c}{b}\bar{\gamma}_{12}{}^{\mathrm{II}} = \bar{\gamma}_{12}{}^{\mathrm{III}} = \bar{\gamma}_{12}\,. \quad (16)$$

From Equations 13 to 16, the transform domain longitudinal shear modulus ($\bar{G}_{12}$) is given as

$$\bar{G}_{12} = \frac{\bar{\tau}_{12}}{\bar{\gamma}_{12}} = \bar{G}_{\mathrm{m}} \frac{(2ab - ac + c^2)(2c\,\bar{G}_{\mathrm{f}}/\bar{G}_{\mathrm{m}} + a - c) + c(a-c)(a+c)}{2a\{(b-c)[2c(\bar{G}_{\mathrm{f}}/\bar{G}_{\mathrm{m}} + a - c] + c(a+c)\}} \quad (17)$$

where $\bar{G}_{\mathrm{f}}$ and $\bar{G}_{\mathrm{m}}$ are the transform domain shear moduli of the fibre and the matrix respectively.

The linear viscoelastic constitutive equation can be derived from the Laplace transform inversion of Equation 1 for which the transform domain moduli $\bar{E}_{11}$, $\bar{E}_{12}$, $\bar{E}_{22}$ and $\bar{G}_{12}$ are substituted.

The calculated results of the moduli for square array ($a = b$) by Equations 2, 3, 11, 12 and 17 are compared with those by Whitney [2], Halpin [4], Tsai [9] and Heaton [12] in Figs. 3 to 6, where $\bar{G}_{\mathrm{f}}/\bar{G}_{\mathrm{m}} = 120$, $\bar{\nu}_{\mathrm{f}} = 0.20$, $\bar{\nu}_{\mathrm{m}} = 0.35$ are assumed. Pretty good coincidences are observed between the authors' calculations and the other investigators' results.

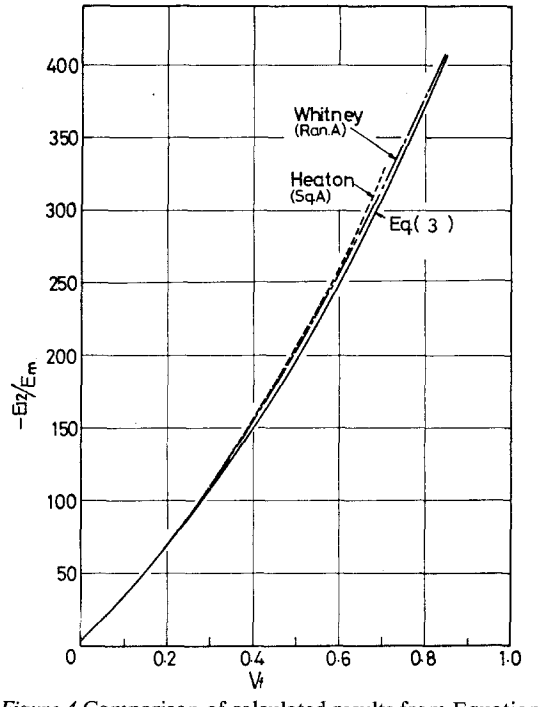

Figure 4 Comparison of calculated results from Equation 3 and from Whitney [2] and Heaton [12].

3. Linear viscoelastic failure criteria

The linear viscoelastic failure criteria are determined from the following two conditions, (1) the proportional limit of the fibre, (2) the bonding failure limit between the fibre and the matrix. It depends on the angle θ between the direction of the fibre and that of the applied stress which limit should be adopted to determine the failure criterion.

3.1. The criterion determined from the fibre proportional limit

The stress of the composite in the longitudinal direction at the proportional limit of the fibre is given by using the law of mixture as follows:

$$\sigma_{11}{}^{*} = V_{\mathrm{f}}\sigma_{\mathrm{f}}{}^{*} + (1 - V_{\mathrm{f}})\sigma_{\mathrm{m}}{}' \quad (18)$$

where $\sigma_{\mathrm{f}}{}^{*}$ is the proportional limit of the fibre and $\sigma_{\mathrm{m}}{}'$ is the stress of the matrix at the proportional limit of the fibre. For uniaxial tension at an angle of θ to the fibre direction, the linear viscoelastic failure stress, $\sigma_{\mathrm{x}}{}^{*}$, becomes

$$\sigma_{\mathrm{x}}{}^{*} = \sigma_{11}{}^{*}/\cos^2\theta = \{V_{\mathrm{f}}\sigma_{\mathrm{f}}{}^{*} + (1 - V_{\mathrm{f}})\sigma_{\mathrm{m}}{}'\}/\cos^2\theta. \quad (19)$$

3.2. The criterion determined from the bonding failure limit

The bonding failure limit between fibre and matrix has usually been given by the critical value of the normal stress or the shear stress on the bonded surface, or by applying the anisotropic yield criterion proposed by Hill. But in the former case, the coupling effect of the normal and shear stresses is neglected, while the physical meaning of debonding is not considered in the latter. To include the coupling effect in the criterion, the bonding failure is assumed to occur when the effective resultant stress

$$\sigma_{\mathrm{eff}} = \sqrt{[(\sigma_{22}{}^{\mathrm{I}})^2 + (\tau_{12}{}^{\mathrm{I}})^2]} \quad (20)$$

on the bonding surface reaches a certain critical value, $\sigma_{\mathrm{eff}}{}^{*}$. The values of $\sigma_{22}{}^{\mathrm{I}}$ and $\tau_{12}{}^{\mathrm{I}}$ in Equation 20 are derived by using the unit cell of Fig. 2b as follows:

$$\bar{\sigma}_{22}{}^{\mathrm{I}} = \left\{1 + \frac{c(a-c)/(b-c)}{\dfrac{2ab - ac + c^2}{b-c} + \dfrac{\bar{E}_{\mathrm{m}}}{\bar{E}_{\mathrm{f}}}\dfrac{2a^2b}{c^2}}\right\}\bar{\sigma}_{22}\,, \quad (21)$$

and

$$\bar{\tau}_{12}^{\mathrm{I}} = \left[\frac{2ab}{a + c + (a - c)\left\{b - c + \dfrac{c(a + c)}{2c(\bar{G}_{\mathrm{f}}/\bar{G}_{\mathrm{m}}) + a - c}\right\}}\right]\bar{\tau}_{12}\,. \tag{22}$$

For $E_{\mathrm{f}} \gg E_{\mathrm{m}}$ and $G_{\mathrm{f}} \gg G_{\mathrm{m}}$, it may be allowed to assume $E_{\mathrm{m}}/E_{\mathrm{f}}$ and $G_{\mathrm{f}}/G_{\mathrm{m}}$ to be constant and independent of the time. Then the stress concentration factors K_1 and K_2 in the physical domain, which are defined by $K_1 = \sigma_{22}^{\mathrm{I}}/\sigma_{22}$ and $K_2 = \tau_{12}^{\mathrm{I}}/\tau_{12}$, become

$$K_1 = 1 + \frac{c(a - c)/(b - c)}{\dfrac{2ab - ac + c^2}{b - c} + \dfrac{E_{\mathrm{m}}}{E_{\mathrm{f}}}\dfrac{2a^2b}{c^2}}\,, \tag{23}$$

$$K_2 = \frac{2ab}{a - c + (a - c)\left\{b - c + \dfrac{c(a + c)}{2c(G_{\mathrm{f}}/G_{\mathrm{m}}) + a - c}\right\}} \tag{24}$$

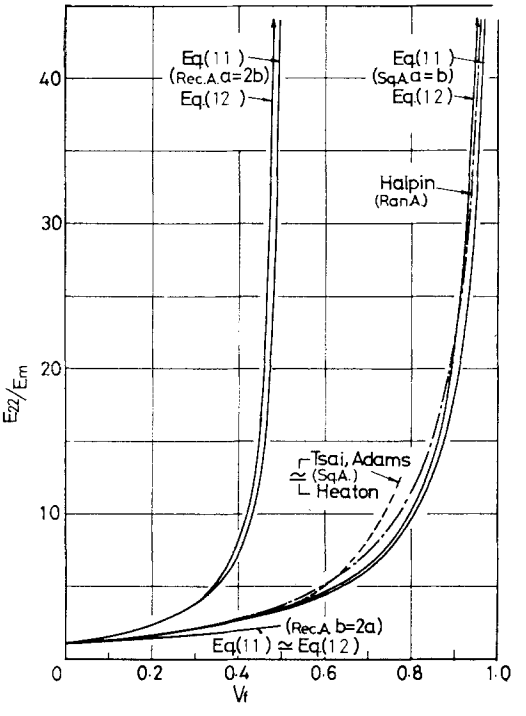

Figure 5 Comparison of calculated results from Equations 11 and 12 and from Halpin [4], Tsai [9] and Heaton [12].

For $K_1 \fallingdotseq K_2$, these can be put $K_1 = K_2 = (K_1 + K_2)/2 \equiv K$. From this approximation the linear viscoelastic failure stress σ_{x}^* for uniaxial tension at an angle of θ to the fibre direction is given by

$$\sigma_{\mathrm{x}}^* = \sigma_{\mathrm{eff}}^*/K \cdot \sin\theta\,. \tag{25}$$

4. Non-linear viscoelastic behaviour

4.1. Constitutive equation in the presence of debonding between fibre and matrix

Let us assume the non-linear viscoelastic constitutive equation in the presence of debonding in the following form,

$$\begin{cases} \epsilon_{11} = C_{11}(\sigma_{11}, t) + C_{12}(\sigma_{22}, t) \\ \epsilon_{22} = C_{21}(\sigma_{11}, t) + C_{22}(\sigma_{22}, t) \\ \gamma_{12} = C_{33}(\tau_{12}, t) \end{cases} \tag{26}$$

where C_{11}, C_{12}, C_{21}, C_{22} and C_{33} are compliance functions of stresses and time. For the longitudinal tensile loading (σ_{11}), both fibre and matrix show the non-linear behaviour before fracture of the composite; the non-linear behaviour of the composite in high stress region will then be predicted by the non-linear behaviour of fibre and matrix. For both transverse loading (σ_{22}) and shear loading (τ_{12}), the composite fracture will occur in a low stress level because of the stress concentration at the matrix-fibre boundary. Hence, the deformation modes of fibre and matrix may be linear until fracture of the composite, and the compliance functions C_{12}, C_{22} and C_{33} will be given by solving elastic problems in the transform domain.

On the assumption that the fibre length is infinite the contact area between the fibre and the matrix may also be regarded as infinite, and the deformations in direction 11 of the fibre and the matrix will show the same value in spite of debonding propagation between them. Hence, the effect of debonding propagation is neglected in determining the compliance functions C_{11} and C_{12}.

4.1.1. $C_{11}(\sigma_{11}, t)$

The stress-strain relations are expressed as follows: for the fibre,

$$\begin{cases} 0 < \sigma_{\mathrm{f}} < \sigma_{\mathrm{f}}^* & \epsilon_{\mathrm{f}11} = \epsilon_{\mathrm{f}}'(\sigma_{\mathrm{f}})\,, \\ \sigma_{\mathrm{f}}^* < \sigma_{\mathrm{f}} < \sigma_{\mathrm{f}}^{**} & \epsilon_{\mathrm{f}11} = \epsilon_{\mathrm{f}}'(\sigma_{\mathrm{f}}) + \epsilon_{\mathrm{f}}''(\sigma_{\mathrm{f}}) \end{cases}, \tag{27}$$

and for the matrix,

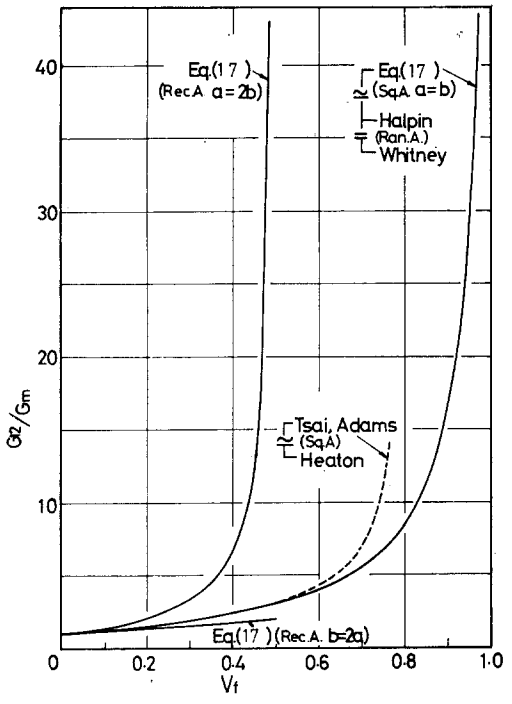

Figure 6 Comparison of calculated results from Equation 17 and from Halpin [4], Tsai [9] and Heaton [12].

$$\begin{cases} 0 < \sigma_m < \sigma_m^* & \epsilon_{m11} = \epsilon_m'(\sigma_m, t), \\ \sigma_m^* < \sigma_m < \sigma_m^{**} & \epsilon_{m11} = \epsilon_m'(\sigma_m, t) + \epsilon_m''(\sigma_m, t) \end{cases} \tag{28}$$

In Equations 27 and 28 the asterisks (*) and (**) denote linear failure stress and fracture stress, respectively, and the primes (′) and (″) linear strain and non-linear strain, respectively. The macroscopic strain (ϵ_{11}) and stress (σ_{11}) in the longitudinal direction are given by

$$\begin{cases} \epsilon_{11} = \epsilon_{f11} = \epsilon_{m11}, \\ \sigma_{11} = V_f\sigma_f + (1 - V_f)\sigma_m. \end{cases} \tag{29}$$

The compliance function (C_{11}) can be determined from the relation $\epsilon_{11} = C_{11}(\sigma_{11}, t)$ by using Equation 29.

4.1.2. C_{21} (σ_{11}, t)

The longitudinal stress-transverse strain relations are expressed as follows:
for the fibre,

$$\begin{cases} 0 < \sigma_f < \sigma_f^* & \epsilon_{f22} = -\nu_f\epsilon_f'(\sigma_f), \\ \sigma_f^* < \sigma_f < \sigma_f^{**} & \epsilon_{f22} = -\nu_f\epsilon_f'(\sigma_f) - \frac{1}{2}\epsilon_f''(\sigma_f), \end{cases} \tag{30}$$

and for the matrix,

$$\begin{cases} 0 < \sigma_m < \sigma_m^* & \epsilon_{m22} = -\nu_m(t)\epsilon_m'(\sigma_m' t) \\ \sigma_m^* < \sigma_m < \sigma_m^{**} & \epsilon_{m22} = -\nu(t)\epsilon_m'(\sigma_m, t) \\ & \quad -\frac{1}{2}\epsilon_m''(\sigma_m, t). \end{cases} \tag{31}$$

In Equations 30 and 31 the Poisson's ratios of the fibre and the matrix in the non-linear region are assumed to be $\frac{1}{2}$. The macroscopic transverse strain (ϵ_{22}) and longitudinal stress (σ_{11}) are written by using law of mixture as

$$\begin{cases} \epsilon_{22} = V_f\epsilon_{f22} + (1 - V_f)\epsilon_{m22}, \\ \sigma_{11} = V_f\sigma_f + (1 - V_f)\sigma_m. \end{cases} \tag{32}$$

The compliance function (C_{21}) can be determined from the relation $\epsilon_{22} = C_{21}(\sigma_{11}, t)$ by using Equation 32.

4.1.3. C_{12} (σ_{22}, t)

As mentioned above, it is assumed that in the transverse loading the composite fracture occurs before linear failure of its components and the longitudinal strains of the fibre and the matrix are equal to each other. Then the compliance function (C_{12}) can be calculated from

$$\overline{C_{12}(\sigma_{22}, t)} = -\frac{\bar{\sigma}_{22}}{\bar{E}_{12}}, \tag{33}$$

where $\bar{E}_{12}$ is given by Equation 3.

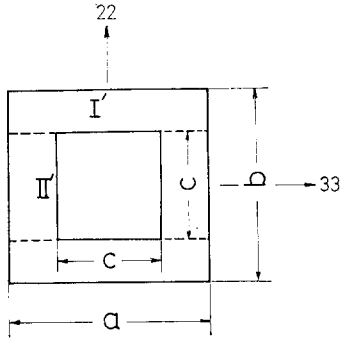

Figure 7 Structural unit cell for the unidirectional fibre reinforced composite where debonding between fibre and matrix occurs.

4.1.4. C_{22} (σ_{22}, t)

For the calculation where debonding between fibre and matrix occurs, the rectangular structural unit cell of Fig. 7 is used. The stress fields in the regions I′ and II′ of the matrix and those in the fibres are assumed to be uniform. When debonding occurs, the fibre acts only as an insert and does not constrain the matrix deformation in the direction of 22. Hence, the effective

modulus of the composite in the direction of 22 can be calculated from the matrix modulus as follows:

$$\bar{E}_{22}' = (1 - c/a)\bar{E}_m \,. \tag{34}$$

The strain compatibility condition under the transverse loading is satisfied by assuming that the longitudinal strains of fibre and matrix are equal to the macroscopic longitudinal strain ($\bar{\epsilon}_{11}$), i.e.,

$$\bar{\epsilon}_{11} = \frac{\bar{\sigma}_{m11}}{\bar{E}_m} - \frac{\bar{\nu}_m \bar{\sigma}_{22}}{\bar{E}_{22}'} = \frac{\bar{\sigma}_{f11}}{\bar{E}_f} \,, \tag{35}$$

where $\bar{\sigma}_{m11}$ and $\bar{\sigma}_{f11}$ denote the longitudinal stresses of matrix and fibre which arise by the constraint in direction 11 between fibre and matrix. The equilibrium condition between these stresses is

$$V_f\bar{\sigma}_{f11} + (1 - V_f)\bar{\sigma}_{m11} = 0 \,. \tag{36}$$

The transverse strain, $\bar{\epsilon}_{22}$, for this case is given by

$$\bar{\epsilon}_{22} = \frac{\bar{\sigma}_{22}}{\bar{E}_{22}'} - \frac{\nu_m \bar{\sigma}_{m11}}{\bar{E}_m} \,. \tag{37}$$

Using Equations 34 to 37 the transverse modulus, $\bar{E}_{22}''$, is obtained from

$$\bar{E}_{22}'' = \frac{\bar{\sigma}_{22}}{\bar{\epsilon}_{22}} = \bar{E}_m \frac{1 - (c/a)}{1 - \bar{\nu}_m^2 \dfrac{V_f\bar{E}_f}{V_f\bar{E}_f + (1 - V_f)\bar{E}_m}} \,. \tag{38}$$

For $\bar{E}_f \gg \bar{E}_m$, $\bar{E}_{22}''$ is simplified to

$$\bar{E}_{22}'' = \frac{1 - (c/a)}{1 - \bar{\nu}_m^2}\bar{E}_m \,, \tag{39}$$

and $\overline{C_{22}(\sigma_{22}, t)}$ is calculated from

$$\overline{C_{22}(\sigma_{22}, t)} = \bar{\sigma}_{22}/\bar{E}_{22}'' \,, \tag{40}$$

with Equation 39.

4.1.5. C_{23} (τ_{12}, t)

Similar to the case of $\bar{E}_{22}'$, the effective shear modulus ($\bar{G}_{12}'$) is determined as

$$\bar{G}_{12}' = \frac{\bar{\tau}_{12}}{\bar{\gamma}_{12}} = [1 - (c/a)]\bar{G}_m \tag{41}$$

and then

$$\overline{C_{33}(\tau_{12}, t)} = \bar{\tau}_{12}/\bar{G}_{12}' \,. \tag{42}$$

4.2. Non-linear constitutive relationship in considering the propagation of debonding

The stress-strain curve in the case of perfect bonding is schematically shown in Fig. 8 by $F'(\sigma)$, and that for complete debonding by $F''(\sigma)$, respectively. The values of the debonding initiating stress and the fracture stress are indicated by σ^* and σ^{**}, respectively. Since the debonding is considered to occur locally and not to propagate instantly throughout the composite at the debonding initiating stress σ^*, the jump of the stress-strain curve from $F'(\sigma)$ to $F''(\sigma)$ will not be observed at this stress. Hence, it is considered that the stress-strain relation deviates gradually from the $F'(\sigma)$ curve with increase of the debonding and finally meets the $F''(\sigma)$ curve at fracture stress σ^{**} as shown by the dashed line in Fig. 8. On the assumption of the linear combination of $F'(\sigma)$ and $F''(\sigma)$, the constitutive relation in considering the propagation of debonding is represented as follows:

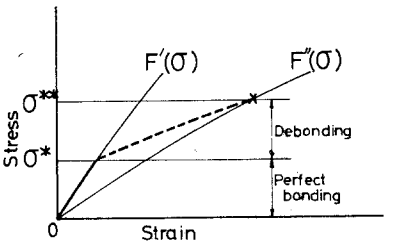

Figure 8 Stress-strain relations in the cases of perfect bonding and debonding.

$$\begin{cases} 0 < \sigma < \sigma^* & \epsilon = F'(\sigma) \\ \sigma^* < \sigma < \sigma^{**} & \epsilon = \dfrac{\sigma^{**} - \sigma}{\sigma^{**} - \sigma^*} F'(\sigma) + \dfrac{\sigma - \sigma^*}{\sigma^{**} - \sigma^*} F''(\sigma) \end{cases}$$

5. Fracture criteria

The fracture conditions are given by the assumption that the composite fracture occurs when either the longitudinal stress or the maximum effective resultant stress of normal and shear stresses on the plane parallel to the fibre reaches its critical value similar to the case of the linear failure criterion.

5.1. Fracture by longitudinal stress

The longitudinal strength of unidirectional brittle fibre reinforced composite can generally be represented by the following law of mixture:

$$\begin{cases} 0 < V_f < V_{fc} & \sigma_{11}{}^{**} = (1 - V_f)\sigma_m{}^{**} \,, \quad (43) \\ V_{fc} < V_f < 1 & \sigma_{11}{}^{**} = V_f\sigma_f{}^{**} + (1 - V_f)\,\sigma_m'' \,, \quad (44) \end{cases}$$

where σ_m'' is the matrix stress corresponding to the fibre fracture strain, and V_{fc} is the critical fibre volume fraction expressed by

$$V_{fc} = (\sigma_m^{**} - \sigma_m'')/(\sigma_f^{**} + \sigma_m^{**} - \sigma_m'') .$$

For the ductile fibre, however, the bonding between the fibre and the matrix prevents "necking" of fibre and, hence, the tensile test result of a single fibre cannot be used as the fibre behaviour in the composite. For the ductile fibre composite, Mileiko [16] has proposed the following modified equation:

$$\sigma_{11}^{**} = V_f\lambda'\sigma_f^{**} + (1 - V_f)\lambda''\sigma_m^{**} , \quad (45)$$

where λ' and λ'' are the functions of fibre volume fraction (V_f). Actual applied results of Equation 45 for the ductile fibre composite show an almost linear relation with V_f. Therefore, the longitudinal fracture criterion is expressed approximately by

$$\sigma_{11}^{**} = V_f\sigma_f^{**} + (1 - V_f)\sigma_m^{**} . \quad (46)$$

5.2. The fracture by the maximum effective resultant stress of normal and shear stresses

The effective resultant stress of normal and shear stresses in the structural unit cell of Fig. 7 is maximum in region II'. Hence, denoting the critical value of effective resultant stress as σ_{eff}^{**}, the fracture condition is given by

$$\sqrt{[(\sigma_{22}^{II'})^2 + (\tau_{12}^{II'})^2]} = \sigma_{eff}^{**} . \quad (47)$$

By defining the stress concentration factor, K', as

$$K' = \frac{\sigma_{22}^{II'}}{\sigma_{22}} = \frac{\tau_{12}^{II'}}{\tau_{12}} = a/(a - c)$$

the fracture stress (σ_x^{**}) in the uniaxial tension with fibre orientation (θ) is expressed as follows:

$$\sigma_x^{**} = \sigma_{eff}^{**}/K' \cdot \sin\theta = \sigma_{22}^{**}/\sin\theta . \quad (48)$$

6. Experimental procedures and results

The tests under creep, relaxation, constant strain-rate and constant load rate conditions are conducted by the biaxial tensile testing machine having a closed loop feedback control system. The temperature during the experiment is kept at 30°C by using an environmental chamber attached to the testing machine. A schematic diagram of the biaxial tensile testing apparatus with various accessories is shown in Fig. 9.

The material used in the experiments is the composite of epoxy resin reinforced unidirectionally by cold-drawn copper wires of 0.8 mm diameter. This composite is produced by pouring the epoxy resin on the copper wires stretched at equal intervals on the glass plate and curing at 60°C for 2 h. The volume fraction of the wire is controlled by changing the intervals between the wires. Test specimens are cut from this composite plate. The uniaxial tensile specimen has a parallel part of 120 mm length and 50 mm

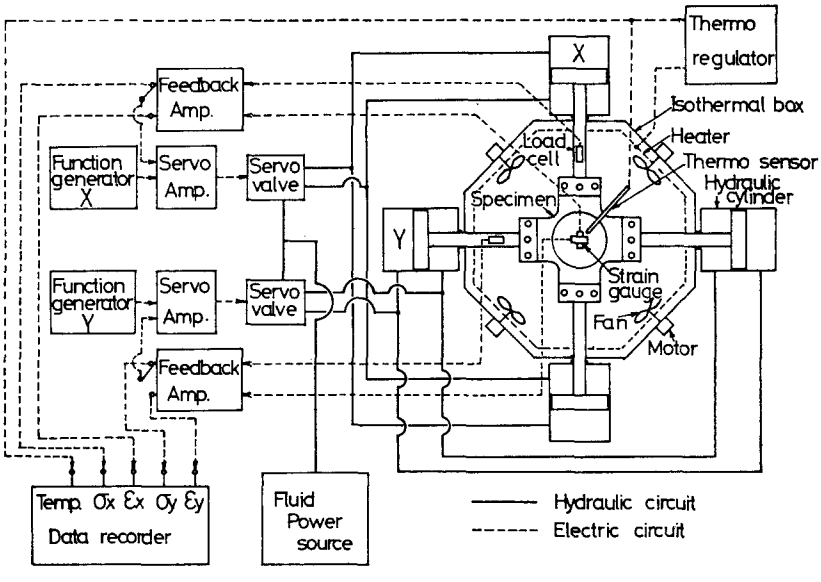

Figure 9 Schematic diagram of testing system.

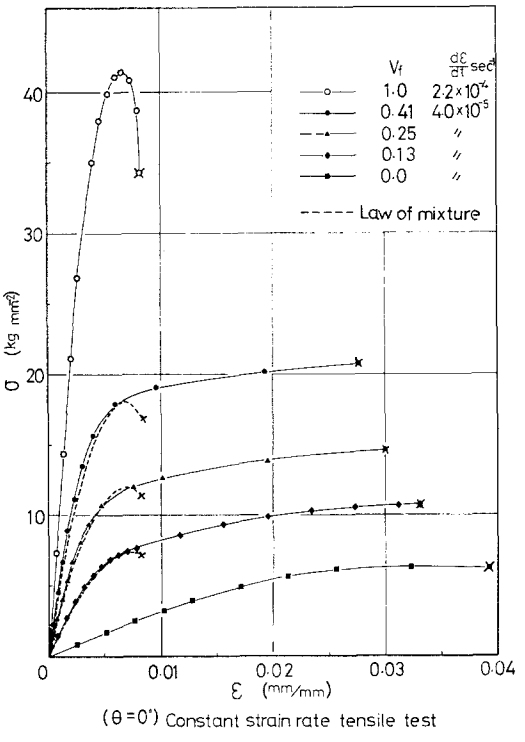

Figure 10 Stress-strain relations under constant strain-rate. ($\theta = 0°$)

breadth, and the biaxial tensile specimen has a square region of 100 mm × 100 mm in the central part.

Experimental results are given in Figs. 10 to 16. Fig. 10 shows longitudinal stress-strain relations under the constant strain-rate tensile tests for copper wire, epoxy resin and their composites with various volume fractions. Figs. 11 and 12 are creep-recovery test results of the composites with fibre volume fraction $V_f = 0.13$ and 0.25, respectively. The relation between the creep compliance and the stress level is plotted in Fig. 13 from the creep test results of the specimen with $V_f = 0.13$ and $\theta = 30°$. The linearity can be clearly seen in low stress levels while non-linearity becomes remarkable for high stress levels. Figs. 14 and 15 show the constant load rate tensile test results of the composites with $V_f = 0.13$ and $V_f = 0.25$, respectively. Results of the biaxial tensile tests under constant stress ratios are given in Fig. 16, where the vertical ordinate expresses the equivalent stress of Mises type.

7. The comparisons between theoretical and experimental results

From the results of the constant strain-rate tensile tests of fibre and matrix and the creep test of matrix, the creep compliances and Poisson's ratios of fibre and matrix are found as follows:

$$J_f(t) = 1/11000 \quad \text{mm}^2\,\text{kg}^{-1}$$
$$\nu_f(t) = 0.33$$
$$J_m(t) = 0.00363 - 0.00025e^{-2.0t} - 0.00050e^{-0.046t}\ \text{mm}^2\,\text{kg}^{-1}$$
$$\nu_m(t) = 0.355.$$

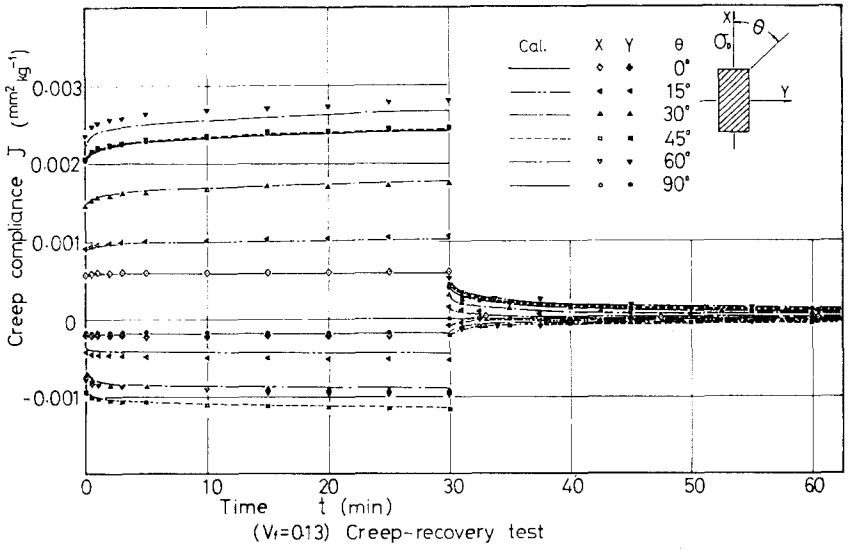

Figure 11 Creep-recovery curves ($V_f = 0.13$).

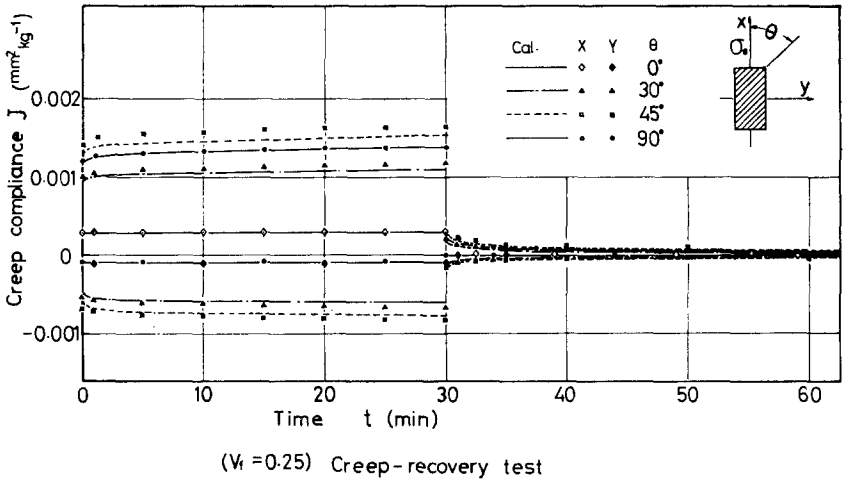

(V_f =0.25) Creep-recovery test

Figure 12 Creep-recovery curves ($V_f = 0.25$).

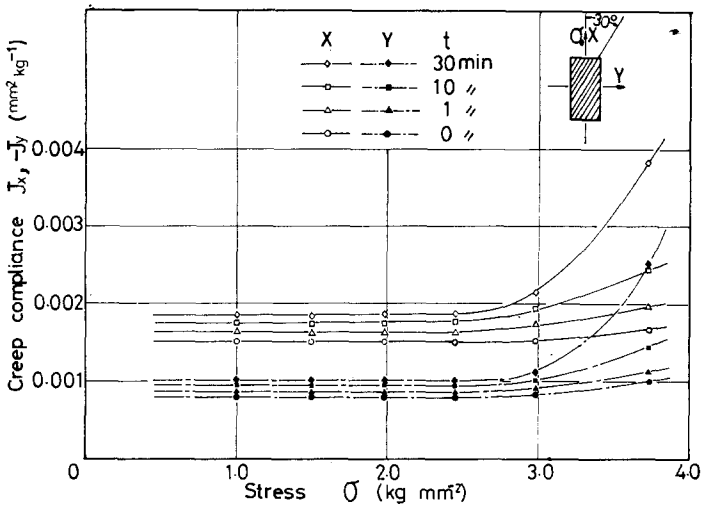

Figure 13 Creep compliance versus stress for various times ($V_f = 0.13$, $\theta = 30°$).

Here the creep compliance of fibre is given as the constant value since the time-dependency in the deformation of the fibre is considered negligible, and times scale in the creep compliance are indicated by minutes. Then the transform domain elastic constants for fibre and matrix become

$$\bar{E}_f = 1/S\overline{J_f(t)} = 11000 \quad (\text{kg mm}^{-2})$$

$$\bar{\nu}_f = S\overline{J_f(t)\nu_f(t)}/S\,\overline{J_f(t)} = 0.33$$

$$\bar{G}_f = \bar{E}_f/2(1 + \bar{\nu}_f) = 4135 \quad (\text{kg mm}^{-2})$$

$$\bar{E}_m = 1/S\,\overline{J_m(t)} = 347\,\frac{(S + 2.0)(S + 0.046)}{(S + 2.17)(S + 0.053)} \quad (\text{kg mm}^{-2})$$

$$\bar{\nu}_m = S\overline{J_m(t)\nu_m(t)}/S\,\overline{J_m(t)} = 0.355$$

$$\bar{G}_m = \bar{E}_m/2(1 + \bar{\nu}_m) = 128\,\frac{(S + 2.0)(S + 0.046)}{(S + 2.17)(S + 0.053)} \quad (\text{kg mm}^{-2}).$$

The constitutive relations calculated by using these transform domain elastic constants and geometrical parameters a, b and c are shown by the lines in Figs. 11, 12, 14 to 16. The calculated stress-strain relations give essentially straight lines in the low stress region and show good

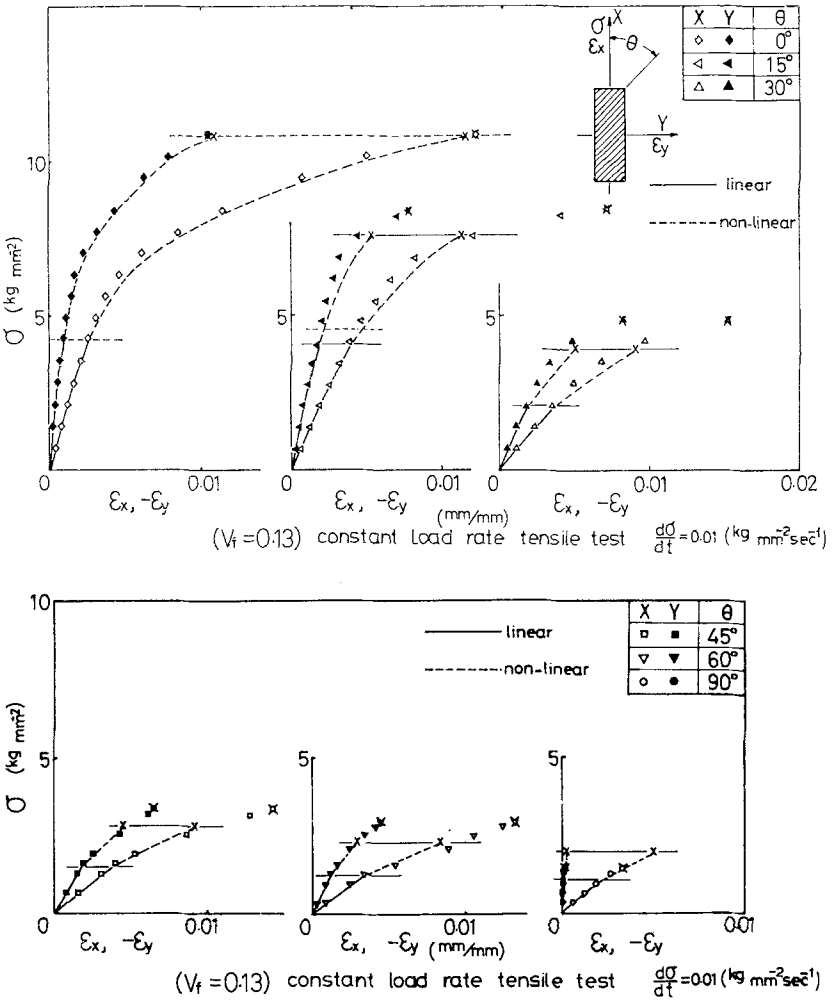

Figure 14 Stress-strain relations under constant stress rate. ($V_f = 0.13$, $d\sigma/dt = 0.01$ kg mm^{-2} sec^{-1})

agreements with the experimental results. The linear viscoelastic failure stress is experimentally defined as the stress point where the gradient of stress-strain curve begins to change abruptly. The relations between the linear viscoelastic failure stress and the fibre orientation are measured for two kinds of uniaxial tensile test specimens of $V_f = 0.25$ and $V_f = 0.13$, and compared with their calculated results by Equations 18 to 20 and 25 as shown in Fig. 17. Fig. 18 shows the comparison between the observed and calculated values of the linear failure stress for the biaxial tensile tests. In these comparisons, the following values are used for the proportional limit of the fibre and the effective resultant stress at the debonding initiation:

$$\sigma_f^* = 27.0 \quad \text{kg mm}^{-2},$$

$$\sigma_{eff}^* = 1.14 \quad \text{kg mm}^{-2}.$$

To calculate the stress-strain relationship of the composite in the non-linear region, the stress-strain curves of fibre and matrix are represented by the following forms:
for the fibre,

$$0 < \sigma_f < 27(\text{kg mm}^{-2})$$

$$\begin{cases} \epsilon_{f11} = \epsilon_f'(\sigma_f) = \dfrac{\sigma_f}{E_f}, \\ \epsilon_{f22} = -\nu_f\epsilon_f'(\sigma_f) = -\dfrac{\nu_f\sigma_f}{E_f}, \end{cases}$$

TABLE I Explanation of stress levels represented by lines.

———	Debonding initiation stress.
——×———	Fracture stress determined from the criterion (5·2).
- - - - - -	At this stress the fibre reaches its proportional limit.
- - - -×- - - -	Fracture stress determined from the criterion (5·1).

$$27 < \sigma_f < 43 (\text{kg mm}^{-2})$$

$$\begin{cases} \epsilon_{f11} = \epsilon_f'(\sigma_f) + \epsilon_f''(\sigma_f) \\ \qquad = \dfrac{\sigma_f}{E_f} - 0.00105 \log \dfrac{43 - \sigma_f}{16}, \\ \epsilon_{f22} = -\nu_f \epsilon_f'(\sigma_f) - \frac{1}{2} \epsilon_f''(\sigma_f) \\ \qquad = -\dfrac{\nu_f \sigma_f}{E_f} + 0.00053 \log \dfrac{43 - \sigma_f}{16}, \end{cases}$$

and for the matrix,

$$0 < \sigma_m < 3.5 (\text{kg mm}^{-2})$$

$$\begin{cases} \bar{\epsilon}_{m11} = \overline{\epsilon_m'(\sigma_m, t)} = \dfrac{\bar{\sigma}_m}{\bar{E}_m}, \\ \bar{\epsilon}_{m22} = -\overline{\nu_m(t)\epsilon_m'(\sigma_m, t)} = -\dfrac{\bar{\nu}_m \bar{\sigma}_m}{\bar{E}_m}, \end{cases}$$

$$3.5 < \sigma_m < 6.3 (\text{kg mm}^{-2})$$

$$\begin{cases} \epsilon_{m11} = \epsilon_m'(\sigma_m, t) + \epsilon_m''(\sigma_m, t) \\ \qquad = \epsilon_m'(\sigma_m, t) - 0.0022 \log \dfrac{6.3 - \sigma_m}{2.8}, \\ \epsilon_{m22} = -\nu_m(t)\epsilon_m'(\sigma_m, t) - \frac{1}{2} \epsilon_m''(\sigma_m, t) \\ \quad = -\nu_m(t)\epsilon_m'(\sigma_m, t) + 0.0011 \log \dfrac{6.3 - \sigma_m}{2.8}. \end{cases}$$

The relations given by the above equations are shown in Fig. 19 by the solid lines. In these relations, the tensile strength of copper wire without necking is assumed to be $\sigma_f^{**\prime} = 43.0$ kg mm^{-2}. The calculated results of the stress-strain curves in non-linear regions are shown in Figs. 14 to 16 by the dashed lines. Figs. 20 and 21 show the comparisons between the calculated and experimental results for the variations of the unidirectional tensile strength with respect to the fibre volume fractions and fibre orientations, respectively. Fig. 22 shows the comparison for the biaxial tensile strength. In these comparisons an experimental average value $\sigma_{eff}^{**} = 3.20$ kg mm^{-2} is adopted for the maximum

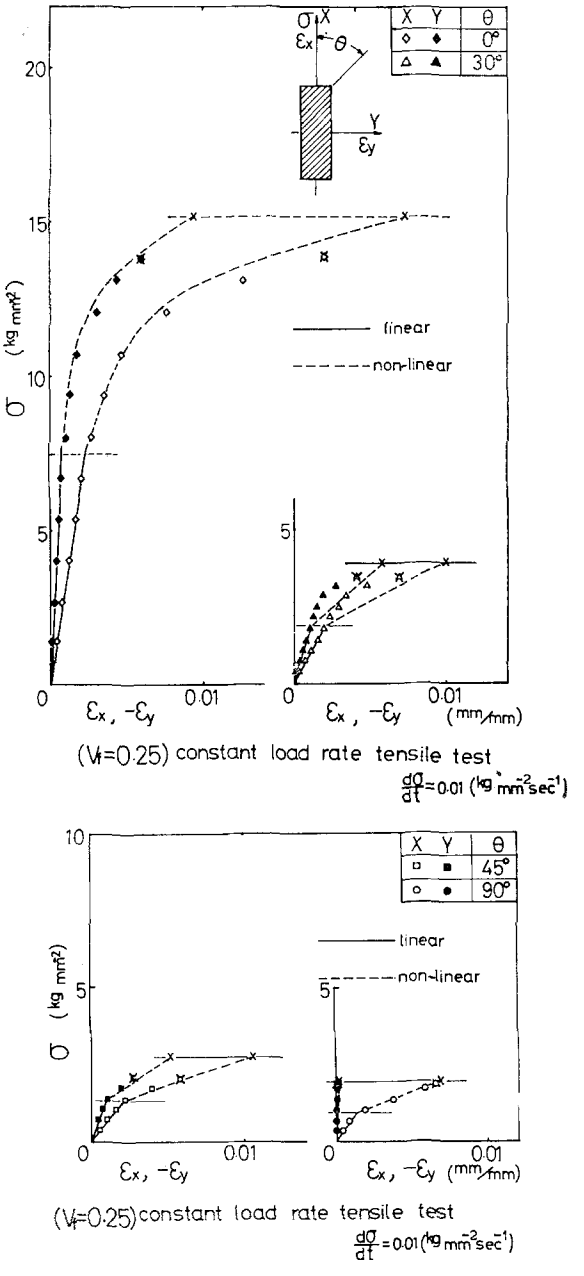

Figure 15 Stress-strain relations under constant stress rate. ($V_f = 0.25$, $d\sigma/dt = 0.01$ kg mm^{-2} sec^{-1})

effective resultant stress σ_{eff}^{**}. The calculated results of linear failure and fracture stress levels are shown in Figs. 14 to 16 by the thin lines (cf. Table I). The changes of the fracture stress with respect to fibre volume fractions and fibre orientations are calculated by Equations 46 and 48, and compared with the experimental

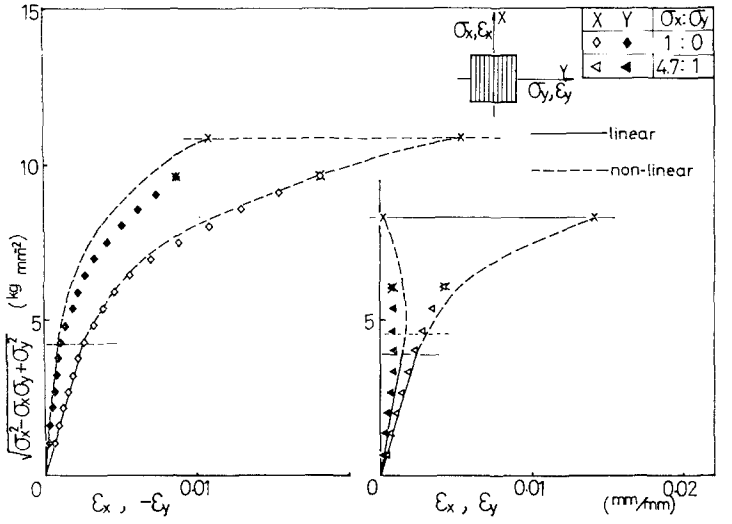

Figure 16 Equivalent stress-strain relations under the biaxial loading with constant stress ratio.

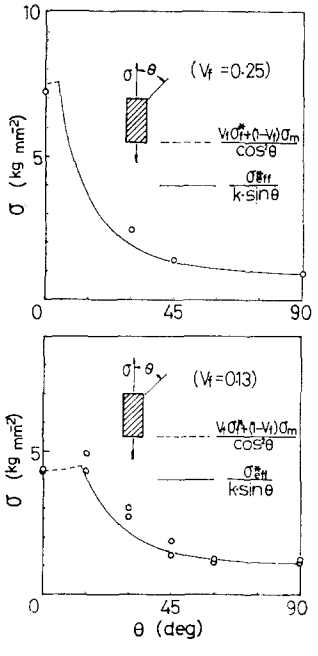

Figure 17 Comparison of calculated and experimental linear viscoelastic failure criteria for uniaxial loading.

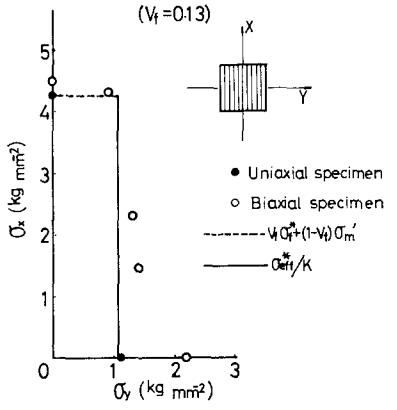

Figure 18 Comparison of calculated and experimental linear viscoelastic failure criteria for biaxial loading.

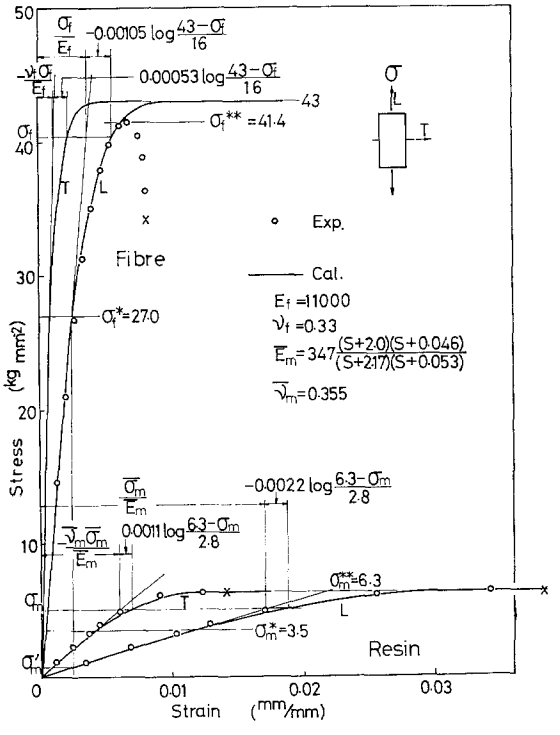

Figure 19 Stress-strain curves of fibre and matrix.

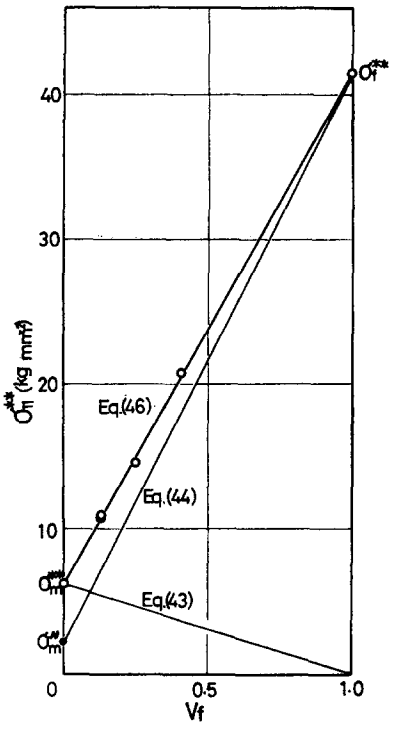

Figure 20 Comparison of calculated and experimental fracture criteria in the fibre direction.

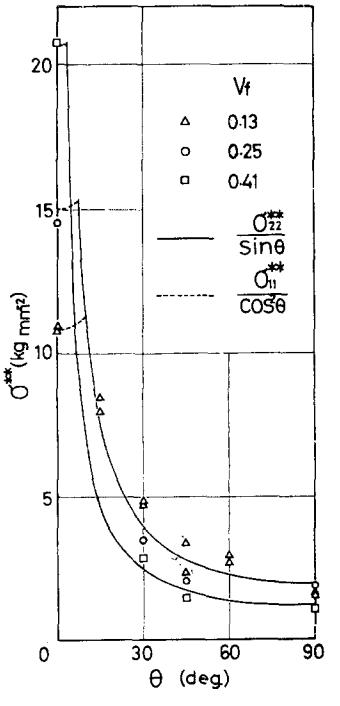

Figure 21 Comparison of calculated and experimental fracture criteria for uniaxial loading.

values by Piehler [17] and those by Cooper [18], Tsai [9] and Jackson [19] in Figs. 23 and 24, respectively. Fairly good coincidences are observed.

8. Conclusions

The mechanical properties of a unidirectional fibre reinforced plastic were investigated theoretically as well as experimentally. The ortho-

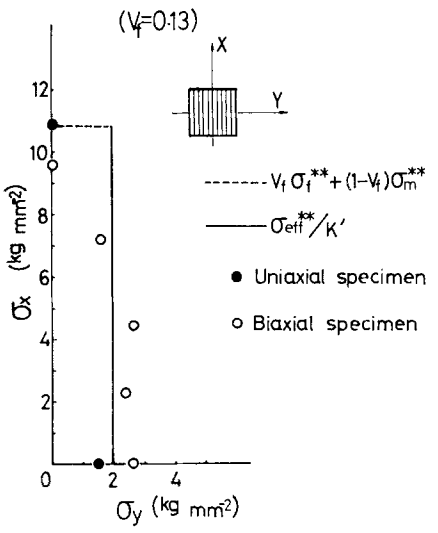

Figure 22 Comparison of calculated and experimental fracture criteria for biaxial loading.

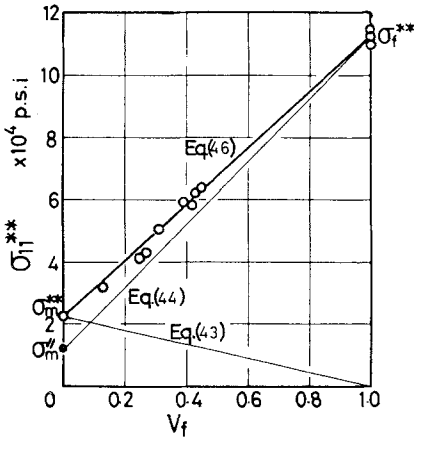

Figure 23 Comparison of calculated results from Equation 46 and experimental results by Piehler [17].

gonal linear viscoelastic constitutive equation was given by the Laplace transform domain elastic constants which were calculated from the law of mixture and a structural unit cell. A linear failure criterion was proposed on the basis of the proportional limit of the fibre and the initiation of debonding between fibre and matrix. The non-linear constitutive relations were derived by considering non-linear properties of the components, and the stress redistribution in matrix on account of debonding between fibre and matrix. Fracture conditions were given by the assumptions that the composite fracture occurs when either the longitudinal normal stress or the maximum effective resultant stress of

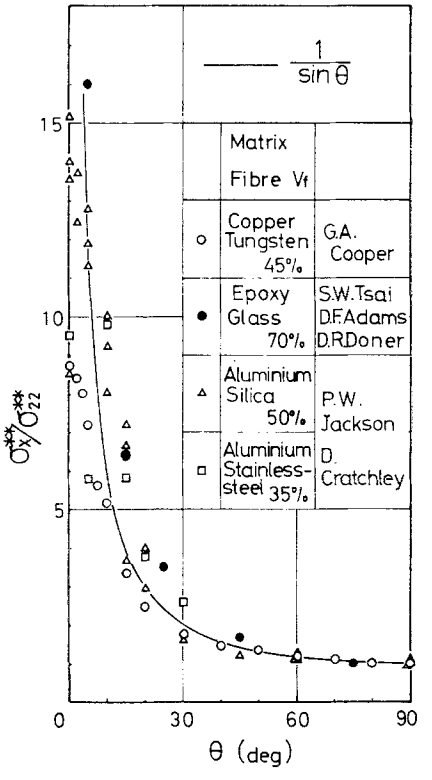

Figure 24 Comparison of calculated results from Equation 48 and experimental results by Cooper [18], Tsai [9] and Jackson [19].

normal and shear stresses on the plane parallel to fibre reach their critical values.

Experimental works under the various loading conditions were made by use of both uniaxial and biaxial specimens of cold drawn copper fibre-epoxy resin composite having various fibre volume fractions and fibre directions. Fairly good agreements were observed between the calculated and experimental results.

References

1. S. W. TSAI, NASA CR. 71 (1964).
2. J. M. WHITNEY and M. B. RILEY, *AIAA J.* **4** (1966) 1537.
3. D. L. MCDANELS, R. W. JECH and J. W. WEETON, *Trans. Met. Soc. AIME* **233** (1965) 636.
4. J. C. HALPIN and S. W. TSAI, AFML TR 67-432 (1967).
5. Z. HASHIN, *J. Mech. Phys. Solids* **13** (1965) 119.
6. Z. HASHIN and B. W. ROSEN, *J. Appl. Mech.* **31**, (1964) 223.
7. R. HILL, *J. Mech. Phys. Solids* **12** (1964) 199.
8. *Idem, ibid* **13** (1965) 189.

9. S. W. TSAI, D. F. ADAMS and D. R. DONER, NASA CR. 620 (1966).
10. D. F. ADAMS, D. R. DONER and R. L. THOMAS, AFML-TR 67-96 (1967).
11. C. H. CHEN and S. CHENG, *J. Comp. Mat.* **1** (1967) 30.
12. M. D. HEATON, *J. Phys, D:Appl. Phys.* **1** (1968) 1039.
13. *Idem, ibid* **3** (1970) 672.
14. P. F. CHEN and J. M. LIN, *Mats. Res. and Stand.* **9** (8) (1969) 29.
15. M. TAKEUCHI and M. KUSUMOTO, *J. Soc. Mat. Sci. Japan* **19** (1970) 750.
16. S. T. MILEIKO, *J. Mater. Sci* **4** (1969) 974.
17. H. R. PIEHLER, *Trans. Met. Soc. AIME* **233** (1965) 12.
18. G. A. COOPER, *J. Mech. Phys. Solids* **14** (1966) 103.
19. P. W. JACKSON and D. CRATCHLEY, *ibid* **14** (1966) 49.

Received 2 August and accepted 28 August 1973.